Title

Do Goethite Surfaces Really Control the Transport and Retention of Multi-Walled Carbon Nanotubes in Chemically Heterogeneous Porous Media?

Journal

Environmental Science and Technology, 50(23)

ISSN

0013-936X

Authors

Zhang, Miaoyue
Bradford, Scott A
Šimůnek, Jirka
et al.

Publication Date

2016-12-06

DOI

10.1021/acs.est.6b03285

Environmental Science & Technology

Article

pubs.acs.org/est

Do Goethite Surfaces Really Control the Transport and Retention of Multi-Walled Carbon Nanotubes in Chemically Heterogeneous Porous Media?

Miaoyue Zhang,[†] Scott A. Bradford,[*,‡] Jirka Šimůnek,[§] Harry Vereecken,[†] and Erwin Klumpp[†]

[†]Agrosphere Institute (IBG-3), Forschungszentrum Jülich GmbH, 52425 Jülich, Germany

[‡]Agricultural Research Service, U.S. Salinity Laboratory, United States Department of Agriculture, Riverside, California 92507, United States

[§]Department of Environmental Sciences, University of California Riverside, Riverside, California 92521, United States

Supporting Information

ABSTRACT: Transport and retention behavior of multi-walled carbon nanotubes (MWCNTs) was studied in mixtures of negatively charged quartz sand (QS) and positively charged goethite-coated sand (GQS) to assess the role of chemical heterogeneity. The linear equilibrium sorption model provided a good description of batch results, and the distribution coefficients (K_D) drastically increased with the GQS fraction that was electrostatically favorable for retention. Similarly, retention of MWCNTs increased with the GQS fraction in packed column experiments. However, calculated values of K_D on GQS were around 2 orders of magnitude smaller in batch than packed column experiments due to differences in lever arms associated with hydrodynamic and adhesive torques at microscopic roughness locations. Furthermore, the fraction of the sand surface area that was favorable for retention (S_f) was much smaller than the GQS fraction because nanoscale roughness produced shallow interactions that were susceptible to removal. These observations indicate that only a minor fraction of the GQS was favorable for MWCNT retention. These same observations held for several different sand sizes. Column breakthrough curves were always well described using an advective-dispersive transport model that included retention and blocking. However, depth-dependent retention also needed to be included to accurately describe the retention profile when the GQS fraction was small. Results from this research indicate that roughness primarily controlled the retention of MWCNTs, although goethite surfaces played an important secondary role.

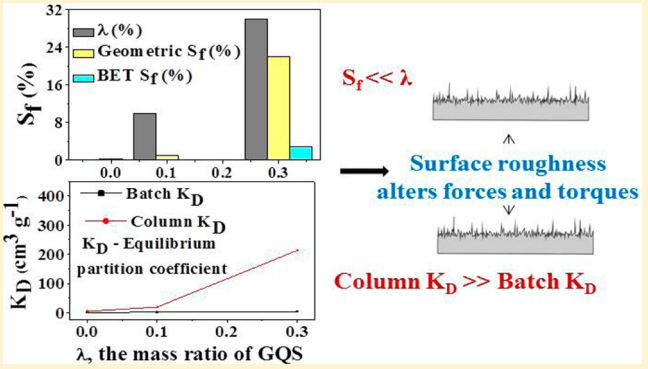

INTRODUCTION

Carbon nanotubes (CNTs) are allotropes of carbon with a needle-shaped nanostructure.[1,2] Single-walled CNTs are individual graphene tubes, whereas multi-walled CNTs (MWCNTs) consist of rolled layers (concentric tubes) of graphene. Carbon nanotubes have unique electrical, chemical, and physical properties that have been utilized in numerous commercial applications.[3,4] Their wide use and lack of disposal regulations are expected to ultimately lead to the release of CNTs into soil and groundwater environments.[5,6] Available literature indicates that CNTs are biologically nondegradable, and they are therefore expected to be very persistent in the environment.[7] Several potential health risks of CNTs in environmental ecosystems have been identified.[8,9] An understanding of factors that influence the transport and fate of CNTs in soils and groundwater is therefore needed to assess the potential risks that CNTs pose to humans and ecosystems.

A number of studies have investigated the transport and retention behavior of CNTs in soils and sand.[6,10−13] Most of this research has been conducted with CNTs that were functionalized to obtain a net negative surface charge in order to enhance the stability of the CNT suspension.[11,14] This research has provided valuable information on the influence of specific physicochemical factors on the fate of CNTs in the environment, including ionic strength and pH, ionic composition, dissolved organic matter and surfactants, input concentration, grain size, and water velocity.[6,10,11,13,15−20] However, most of these studies have only measured CNT breakthrough curves and have not determined retention profiles that are needed to achieve mass balance and to better determine retention mechanisms.[11,21] Furthermore, high CNT concentrations have commonly been employed that are not environmentally relevant.[13,15,17,18,22] No research studies have systematically examined the influence of soil chemical

Received: July 1, 2016
Revised: October 11, 2016
Accepted: October 27, 2016
Published: October 27, 2016

DOI: 10.1021/acs.est.6b03285
Environ. Sci. Technol. XXXX, XXX, XXX−XXX

heterogeneities on the transport and fate of functionalized CNTs.

Iron (Fe) and aluminum (Al) oxyhydroxides are the most common source of surface charge heterogeneity in natural aquatic environments. Both Fe and Al oxyhydroxides are amphoteric minerals that have relatively high points of zero charge. The zero point of charge for Fe and Al oxyhydroxides is reported to be 7.5 and 9,[23] respectively. These minerals adsorb protons and acquire a net positive surface charge in aquatic environments that are below their zero point of charge. In contrast, common silica minerals exhibit a net negative surface charge at ambient pH values because of their lower zero point of charge.[24] Natural porous media therefore often exhibit surface charge heterogeneity. If functionalized CNTs are negatively charged, then the electrostatic interaction is expected to be "favorable" on positively charged Fe and Al hydroxyoxides and "unfavorable" on negatively charged silica minerals under neutral pH conditions. The influence of chemical heterogeneity on the transport and retention of colloids, microbes, and other engineered nanoparticles has been previously studied by using various combinations of untreated and iron oxide-coated quartz sand.[25−27] Results demonstrate that increasing the iron oxide-coated sand fraction (chemical heterogeneity) increases the amount of retention, presumably due to attachment onto iron oxide-coated sand. However, the potential confounding roles of roughness have not been considered in these studies.

A number of experimental and theoretical studies have demonstrated the important role of roughness on colloid and nanoparticle retention.[28,29] Nanoscale roughness on macroscopically "unfavorable" surfaces locally reduces the energy barrier height to create regions where particle interaction in a primary minimum is "favorable".[28,30] The combination of nanoscale roughness and Born repulsion on a macroscopically "favorable" surface also creates a shallow primary minimum where interacting particles are susceptible to diffusive or hydrodynamic removal.[30,31] Consequently, the question arises whether iron oxide-coated surfaces are truly favorable to CNT retention.

Batch and column experiments are common approaches to study colloid retention in porous media.[32] Some researchers have attempted to use batch experiments to predict the retention behavior of colloids and nanoparticles in packed columns[33,34] because batch studies are generally more simple, quick, and less costly than packed column experiments. However, distinct differences in the amount of colloid retention on clean quartz sand have been reported for various sized colloids and solution chemistries.[32] In particular, much greater amounts of colloid retention occur in packed column than batch systems, especially for larger colloids and lower ionic strength (IS) conditions, due to differences in lever arms associated with applied hydrodynamic and resisting adhesive torques at microscopic roughness locations and grain−grain contacts;[32] for example, lever arms are constant in column systems whereas they continuously change in mixed batch systems. It is still unclear whether differences in colloid retention in batch and column systems will decrease under electrostatically favorable conditions that occur on iron oxide-coated surfaces. If so, then batch experiments could potentially be employed to predict colloid transport and retention behavior at the column scale on electrostatically favorable surfaces.

A number of mathematical models have been developed to simulate the transport and retention of colloids and nanoparticles in soils and groundwater.[35−40] These models typically consider advective and dispersive transport but differ in their description of retention processes.[11,40,41] The simplest model employs filtration theory to describe first-order irreversible colloid retention.[39,42,43] Further levels of model complexity are added by considering other processes such as release, retention on multiple kinetic sites, time-dependent blocking or ripening behavior, and depth-dependent retention processes.[11,12,40,41,44] Model analysis of experimental data provides valuable information on processes that control colloid retention by allowing various hypotheses to be tested.[45] Additional modeling studies are especially warranted in chemically heterogeneous porous media (i.e., mixtures of quartz sand and iron oxide-coated quartz sand). In this case, multiple kinetic retention sites are fully justified, and it may be possible to separately study and predict retention parameters for "favorable" and "unfavorable" sites.

The overall objective of this study was to investigate and simulate the transport and retention of MWCNTs at an environmentally relevant concentration (1 mg L^{-1}) in both batch and column experiments in chemically heterogeneous porous media with different mass ratios of quartz sand (QS) and goethite-coated quartz sand (GQS). Several different sand grain sizes were considered in these experiments. Measured breakthrough curves (BTCs) and retention profiles (RPs) were simulated using models of increasing complexity. Our analysis provides an improved understanding of the relative importance of roughness and electrostatically "favorable" surfaces on MWCNT retention in chemically heterogeneous porous media.

MATERIALS AND METHODS

Carbon Nanotubes. Radioactively (^{14}C) labeled MWCNTs were prepared by catalytic chemical vapor deposition using ^{14}C-benzene as feedstock gas (Bayer Technology Services GmbH, Leverkusen, Germany). The synthesis, functionalization, and characterization of these functionalized MWCNTs were previously described.[11,12] The MWCNTs have a median diameter of 10−15 nm, a median length of 200−1000 nm,[46] an average hydrodynamic diameter of approximately 180 nm (determined by dynamic light scattering, Malvern Instruments GmbH, Herrenberg, USA), and a specific density of 1.641 g cm^{-3}.[47] Well-dispersed stock suspensions of MWCNTs were prepared in 1 mM KCl by ultrasonicating for 15 min at 65 W using a cup horn sonicator (Branson Sonifier W-250, Danbury, CT, U.S.A.). These stock suspensions were ultrasonicated (for 10 min) a second time immediately before use in batch or column studies. The concentration of ^{14}C-labeled MWCNTs was determined using a PerkinElmer (Rodgau, Germany) liquid scintillation counter (LSC). LSC is the measurement of activity associated with a radioactive sample. The unit of LSC is Becquerel (Bq), and the specific radioactivity of the functionalized MWNTS was 3.2 MBq mg^{-1}.

Preparation of Porous Media. Three highly uniform sand sieve size fractions of quartz sand (QS) were used in the experiments. The median grain size of these sieved size fractions was 240, 350, and 607 μm. These QS were purified following a protocol in the literature.[11] Stable, high density, goethite-coated quartz sand (GQS) was prepared using the procedure of Scheidegger et al.[48] The surface roughness and distribution of goethite coating on the QS and GQS were imaged using a scanning electron microscope (SEM). The Brunauer−Emmett−Teller (BET) surface area[49] and iron concentration of the QS and GQS were also measured. Chemically heterogeneous porous medium was prepared by combining a known mass fraction of GQS (λ) with QS. Values of λ = 0, 0.1, and 0.3 were selected to be

DOI: 10.1021/acs.est.6b03285
Environ. Sci. Technol. XXXX, XXX, XXX−XXX

consistent with reported ranges in the literature.[27,50] Section S1 of the Supporting Information (SI) provides details.

Interaction Energy Calculations. The approach of Bradford and Torkzaban[30] was used to calculate the total interaction energy (Φ) of a spherical colloid with similar properties to MWCNTs on QS and GQS in 1 mM KCl solution. These calculations allowed consideration of selected roughness properties on the sand surface and employed a Hamaker constant of 9.8×10^{-21} J[51] and a hydrodynamic diameter of 180 nm to be consistent with MWCNTs. Zeta potentials of MWCNTs, crushed QS, and goethite particles in 1 mM KCl solution were also determined using a Zetasizer Nano (Malvern Instruments GmbH, Herrenberg, Germany. Details pertaining to these calculations are given in Section S2 of the SI.

Batch Experiments. Batch experiments were conducted using MWCNTs and two different sizes (350 and 607 μm) of QS and GQS. In accordance with the Organization for Economic Cooperation and Development (OECD) Guideline 106,[52] batch sorption experiments were carried out under quasi-equilibrium conditions[33] by adding 20 mL of ^{14}C-labeled functionalized MWCNT suspensions of different concentrations (0−1 mg L^{-1} of MWCNT in 1 mM KCl) to 1 g of QS or GQS in a centrifuge tube (50 mL). The tubes were continuously mixed using an overhead shaker for 24 h. Preliminary experiments revealed that this duration was sufficient for sorption equilibrium. After removing the suspension of MWCNT, the sorbents (QS or GQS) were dried in an oven at 50 °C and combusted by using a biological oxidizer (OX 500, R.J. Harvey Instrumentation Corporation, Tappan, NY, U.S.A.). The emerging $^{14}CO_2$ was dissolved in vials filled with a scintillation cocktail (Oxisolv, MERCK KGAA, Darmstadt, Germany), and the ^{14}C concentration of MWCNTs adsorbed to the sorbents was determined using the LSC. The concentration of MWCNTs in the supernatant filled with the scintillation cocktail (5 mL, Insta-Gel Plus, PerkinElmer, Rodgau, Germany) before and after the sorption experiments was also measured with the LSC so that the total mass balance of MWCNTs could be determined. All the sorption experiments were performed in triplicate. Blank experiments were conducted to verify that minimal sorption of ^{14}C-labeled MWCNTs occurred to the wall of the centrifuge tube and the air−water interface. Nearly complete mass balance was achieved in the blank experiments (>99%).

Column Transport Experiments. Chemically heterogeneous porous media (QS and GQS mixtures) were incrementally wet packed (deionized water) into stainless steel columns (3 cm in inner diameter and 12 cm in length) equipped with a stainless steel plate (1 mm openings) and a polytetrafluoroethylene (PTFE) mesh (100 or 200 μm openings) at the column bottom to support the porous media. The column was connected to a pump (MCP V 5.10, Ismatec SA, Glattbrugg, Switzerland) on the inlet side with the flow direction from the bottom to the top of the column at a Darcy velocity of 0.72−0.75 cm min^{-1}. This Darcy velocity is consistent with rapid sand filtration studies, flow near injection/extraction wells, and other published column studies examining colloid and nanoparticle transport and fate.[11,53] Approximately 30 pore volumes (PV) of background electrolyte solution (1 mM KCl) were passed through the column before conducting the transport experiments. A nonreactive tracer (1 mM KBr, approximately 90 mL and 2.6 PVs) pulse was injected into the column to characterize the hydraulic conditions (porosity and dispersivity), followed by elution with the same particle-free electrolyte solution (approximately 3.2 PVs). Effluent solutions of bromide were collected using a fraction collector (FoxyJr., Teledyne Isco, Inc., Lincoln, NE, U.S.A.) every 30 s (e.g., approximately 2.5 mL per vial) and measured using a high-performance liquid chromatography (HPLC) (STH 585, Dionex, Sunnyvale, CA, U.S.A.) equipped with a UV-detector (UV2075, Jasco, Essex, U.K.). The same procedure was repeated when MWCNT suspensions were applied. A relatively low input concentration of MWCNT (1 mg L^{-1}) was selected for all column experiments to be consistent with environmentally relevant scenarios.[5,54] The effluent concentrations of MWCNTs were measured using the LSC. After recovery of the breakthrough curve, the sand in the packed column was excavated in approximately 0.5−1 cm thick increments, dried, and then homogenized using a mill. Similar to the sorption experiments, the crushed sands were combusted by using a biological oxidizer and measured using the LSC to determine the MWCNTs retained in the column packing. The total mass balance of MWCNTs in the effluent and retained in the sand was determined from this information. All column experiments were replicated and exhibited good reproducibility.

NUMERICAL MODELING

The HYDRUS-1D code[55] was used to simulate the one-dimensional transport of MWCNTs with the advection-dispersion equation (ADE) and two kinetic retention sites:[56,57]

$$\theta\frac{\partial C}{\partial t} + \rho\frac{\partial S_1}{\partial t} + \rho\frac{\partial S_2}{\partial t} = \theta D\frac{\partial^2 C}{\partial x^2} - q\frac{\partial C}{\partial x} \quad (1)$$

where θ is volumetric water content [L^3L^{-3}, where L denotes units of length], C is MWCNT concentration in liquid phase [NL^{-3}, where N denotes number], t is the time [T, where T denotes units of time], ρ is the bulk density of the porous matrix [ML^{-3}, where M denotes units of mass], x is the spatial coordinate [L], D is the hydrodynamic dispersion coefficient [L^2T^{-1}], q is the Darcy velocity [LT^{-1}], and S_1 and S_2 [NM^{-1}] are the solid-phase concentrations of MWCNTs on retention sites 1 and 2, respectively. The solid phase mass balance on sites 1 and 2 are given as

$$\rho\frac{\partial S_1}{\partial t} = \theta\psi_1 k_{sw1} C - \rho k_{rs1} S_1 \quad (2)$$

$$\rho\frac{\partial S_2}{\partial t} = \theta\psi_2 k_{sw2} C - \rho k_{rs2} S_2 \quad (3)$$

where subscripts 1 and 2 on parameters denote the site, k_{sw1} and k_{sw2} [T^{-1}] are the first-order retention rate coefficients, k_{rs1} and k_{rs2} [T^{-1}] are the first-order release rate coefficients, and ψ_1 and ψ_2 [-] are dimensionless functions that account for time or depth-dependent retention. The total solid-phase concentration (S; NM^{-1}) is equal to the sum of S_1 and S_2.

Three model formulations for MWCNT retention were considered in this work. The first model (M1) considers retention only on Site 1 (k_{sw2} = 0) and time-dependent Langmuirian blocking by setting ψ_1 equal to

$$\psi_1 = 1 - \frac{S_1}{S_{max1}} \quad (4)$$

where S_{max1} [NM^{-1}] is the maximum solid phase concentration on Site 1. This model accounts for retention of MWCNTs on both QS and GQS using a single retention site. The percentage of the solid surface area that is favorable for MWCNT retention (S_f) can be determined from S_{max1} as[32]

DOI: 10.1021/acs.est.6b03285
Environ. Sci. Technol. XXXX, XXX, XXX−XXX

$$S_f = 100 \times \frac{A_c \rho S_{max1}}{(1-\gamma)A_s} \quad (5)$$

where γ [-] is the porosity of a monolayer packing of MWCNTs on the solid surface that is equal to 0.5,[58] A_c [L^2N^{1-}] is the effective cross-section area per MWCNT, and A_s [L^{-1}] is the solid surface area per unit volume. Details on parameters are given in Section S3 of the SI.

The M2 model separately accounts for retention and blocking of MWCNTs on QS (Site 1) and GQS (Site 2) sites using eqs 2 and 3, respectively, by defining ψ_2 in an analogous fashion to ψ_1 (e.g., S_1 and S_{max1} in eq 4 are replaced with S_2 and S_{max2}, respectively). The M3 model considers retention and time-dependent blocking on Site 1 using eqs 2 and 4 and depth-dependent retention on Site 2. In this case, the value of ψ_2 was defined as

$$\psi_2 = \left(\frac{d_{50} + x}{d_{50}}\right)^{-\beta} \quad (6)$$

where d_{50} [L] is the median grain size of the porous media, β [-] is a fitting parameter which controls the shape of the retention profile. We set the value of $\beta = 0.765$ based on reported results for MWCNTs.[11,12]

RESULTS AND DISCUSSION

SEM Images. Figure S1 shows SEM images of QS and GQS at several different magnifications. These images clearly show the complex surface topography of the sand grain surfaces. Different amounts and heights of roughness are found over the surface of both QS and GQS. EDX measurement was used to confirm the presence of goethite on the GQS. The SEM images indicate that the goethite coating exhibits a wide distribution of sizes, shapes, and density on the surface of GQS. Consequently, quantitative determination of the goethite surface coverage was not possible. However, Wang et al.[50] reported that a similar goethite coating technique produced a 75% surface coverage on the sand. Similarly, Duschl et al.[59] reported that our goethite coating technique produced a high goethite surface density of 6 to 27 particles per μm^2. Collectively, the literature and Figure S1 indicate a high density of goethite particles coated the GQS. This was further confirmed by measurement of high iron concentrations following acid digestion of the GQS (Table S1).

Interaction Energies. The average zeta potentials of MWCNTs, crushed quartz sand, and goethite particles in 1 mM KCl solution were measured to be −40.2, −63.6, and 10.2 mV, respectively. Consequently, the electrostatic interaction between the MWCNTs and quartz is unfavorable, whereas that between MWCNTs and goethite is favorable. However, Φ also depends on van der Waals and Born interactions. Figure S2 presents plots of Φ as a function of separation distance (h) when a spherical colloid, with properties similar to MWCNTs, approaches the surface of QS and GQS in 1 mM KCl when the sand surface has a uniform roughness height of 50 nm and roughness fraction of 0.5%, 1%, 2.5%, and 5%. The energy barrier to the primary minimum is present and absent on QS and GQS, respectively, as expected based on electrostatics. However, the height of the energy barrier and the depth of the primary minimum is a strong function of the roughness fraction. A decrease in the roughness fraction produces a rapid decrease in the energy barrier on the QS and the magnitude of the primary minimum on the GQS. The kinetic energy model predicts that colloids could diffuse over these small energy barriers on the QS and out of these shallow primary minimum on the GQS as a result of surface roughness.[29,30] Consequently, these observations indicate that QS and GQS may not be completely "unfavorable" and "favorable", respectively, as expected based on only electrostatic considerations.

Batch Experiments. Batch experiments were conducted to quantify the sorption behavior of MWCNTs onto two grain sizes (350 and 607 μm) of QS and GQS. Replicate batch experiments exhibited good reproducibility and mass balance. Figure 1 shows

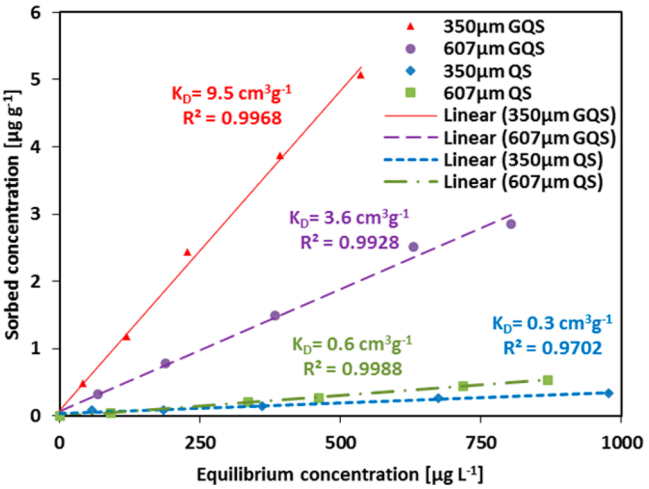

Figure 1. Linear sorption isotherms for MWCNTs on QS or GQS having grain sizes of 350 and 607 μm. The electrolyte solution was 1 mM KCl.

the sorption isotherms. The linear equilibrium sorption model ($S = K_D C$, where K_D [L^3 M^{-1}] is the equilibrium partition coefficient)[52] provided an excellent description of all isotherm data sets, with the coefficient of linear regression (R^2) always greater than 0.97. The sorption behavior over this concentration range was therefore completely characterized by values of K_D, i.e., the slope of the linear isotherm.

Values of K_D were much larger on GQS (K_D = 9.5 and 3.6 cm^3 g^{-1} on 350 and 607 μm sand, respectively) than QS (K_D = 0.3 and 0.6 cm^3 g^{-1} on 350 and 607 μm sand, respectively). This result is expected because the electrostatic interaction between the negatively charged MWCNTs (i.e., carboxylate groups, $-COO^-$) and the positively charged GQS ($Fe-OH^{2+}$) is attractive, whereas it is repulsive for the negatively charged QS.[60,61] Figure S2 also confirms that statement and demonstrates that the significant amounts of roughness shown in Figure S1 will decrease and increase the MWCNT adhesive interaction between GQS and QS, respectively. The value of K_D also dramatically increased with a decrease in the grain size of the GQS because of a corresponding increase in the specific surface area (Table S1). This grain size effect was not observed for QS. In contrast to GQS, the value of K_D on QS is controlled by small amounts of nanoscale roughness and chemical heterogeneity that locally reduces or eliminates the energy barrier (Figure S2).[29,30,32] One plausible explanation for the slight increase in K_D with increasing grain size of QS is due to differences in the amount and distribution of these nanoscale heterogeneities (Figure S1 and Table S1).

Effect of Goethite Coating on MWCNT Transport. Figure 2a and b presents BTCs and RPs, respectively, for MWCNTs in various mass ratios of uncoated and goethite-coated quartz sand (λ = 0, 0.1 and 0.3). The BTCs are plotted as

DOI: 10.1021/acs.est.6b03285
Environ. Sci. Technol. XXXX, XXX, XXX−XXX

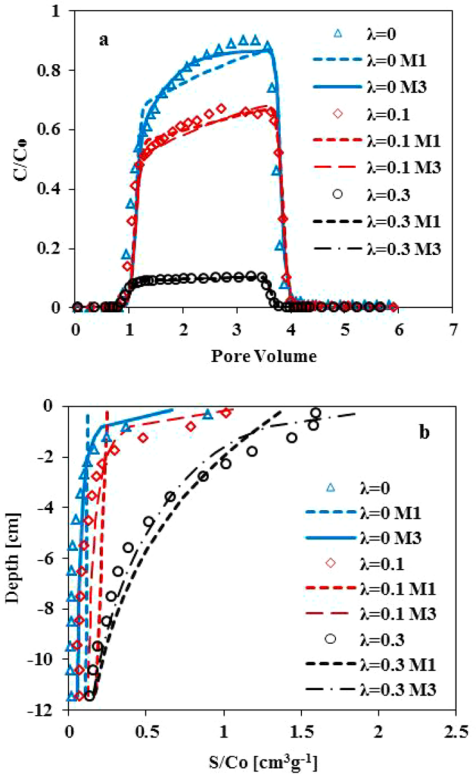

Figure 2. Experimental and estimated breakthrough curves (a) and retention profiles (b) for MWCNTs under different mixing mass ratios (λ). The Darcy velocity was 0.72−0.75 cm min^{-1}. The grain size of the sand was 350 μm.

the normalized effluent concentration (C/C_0, where C_0 is the influent suspension concentration) of MWCNTs versus pore volumes. The RPs are given as normalized solid-phase concentration (S/C_0) against column depth. The experimental conditions and mass balance information are presented in Table 1. The total mass balance (M_{total}) for MWCNTs in these experiments was very good (>90.7%). The MWCNT effluent mass balance (M_{eff}) strongly decreased from 79.6% to 9.7% (Table 1) as λ increased from 0 to 0.3. Similarly, the MWCNT solid-phase mass balance (M_{solid}) increased from 16.3% to 82.8% as λ increased from 0 to 0.3. As expected from batch experiments, these observations reflect the increasing amounts of favorable electrostatic interactions between negatively charged MWCNTs and positively charged goethite as λ increases.

Mathematical model studies were conducted to investigate the relationship between column retention and batch sorption parameters for MWCNTs. The M1 model was initially employed to describe the BTCs shown in Figure 2a for the various sand mixtures. Table 2 provides a summary of fitted M1 model parameters (k_{sw1}, k_{rs1}, and S_{max1}) and separate R^2 values for BTCs and RPs. Simulations for the M1 model are shown in Figure 2, and R^2 values for BTCs were always very good (R^2> 0.96). Fitted M1 model values of k_{sw1} and k_{rs1} were subsequently employed to determine column values of $K_D = \frac{\theta k_{sw1}}{\rho k_{rs1}}$.[32,42] Batch K_D values for these same sand mixtures were determined as a linear combination of components equal to $(1 - \lambda)\ K_{QS} + \lambda\ K_{GQS}$, where K_{QS} and K_{GQS} are batch K_D values for QS and GQS (cf. Figure 1), respectively. Column and batch values of K_D are given in Table 2. Note that column values of K_D are always much larger than batch values, and this difference increased with λ (nearly 2 orders of magnitude higher when λ = 0.3). Clearly, the batch results had little relevance in predicting column scale retention even when the electrostatically favorable fraction was relatively high (λ = 0.3).

Others have observed a similar inconsistency between batch and column retention parameters.[29,32,62,63] Torkzaban and Bradford[29] provided a detailed explanation for differences in colloid retention parameters in batch and column studies. In brief, the amount of retention in batch and column experiments depends on the forces and torques that act on MWCNTs near the porous medium surface.[29,32] The torque balance between applied hydrodynamic (T_H) and resisting adhesive (T_A) torques is not continuously satisfied in a well-mixed batch system because changes in the flow direction alter the lever arms. Conversely, the torque balance in the column system is constantly satisfied ($T_H \leq T_A$) at microscopic roughness locations (Figure S1) and grain−grain contacts that reduce the lever arm for T_H and increase the lever arm for T_A. Greater amounts of MWCNT retention are therefore expected in the column than the batch system for similar values of adhesive, hydrodynamic, buoyancy, and diffusive forces. In other words, different mechanisms of MWCNT retention occur in batch and column systems. Only attachment processes contribute to MWCNT retention in the batch system, whereas attachment and surface straining processes (dependent on the grain surface topology) operate in the column system. Note that this analysis does not consider the potential influence of pore straining that may occur in column systems when the porous medium has wider ranges in grain- and pore-size distributions.

Fitted values of k_{sw1} showed a nonlinear dependency on λ. In particular, k_{sw1} slightly increased as λ increased from 0 to 0.1 but dramatically increased when λ increased from 0.1 to 0.3. This result is consistent with bacteria transport studies in various fractions of iron oxide-coated sands,[25,26] but a linear increase in k_{sw1} with λ has been reported for nanoparticles.[27,64] This discrepancy is likely related to differences in the size of the

Table 1. Experimental Conditions, Hydraulic Parameters, and Mass Balance Information for All Column Experiments[a]

λ	d_{50} [μm]	ρ [g cm^{-3}]	q [cm min^{-1}]	*Disp.* [cm]	Porosity	M_{eff} [%]	M_{solid} [%]	M_{total} [%]
0	350	1.69	0.73	0.025	0.41	79.6	16.3	95.9
0.1	350	1.7	0.72	0.033	0.4	60.6	30.1	90.7
0.3	350	1.71	0.75	0.036	0.43	9.7	82.8	92.5
0.1	240	1.63	0.75	0.036	0.43	2.4	94.2	96.6
0.1	350	1.7	0.72	0.033	0.4	60.6	30.1	90.7
0.1	607	1.29	0.73	0.033	0.47	76.0	17.7	93.7

[a]IS was 1 mM KCl. The input concentration of MWCNT was 1 mg L^{-1}. ρ is the bulk density. *Disp.* is the estimated longitudinal dispersivity. M_{eff} is the effluent percentage of MWCNTs recovered from the column experiment. M_{solid} is the retained percentage of MWCNTs recovered from the column experiment. M_{total} is the total percentage of MWCNTs recovered from the column experiment.

DOI: 10.1021/acs.est.6b03285
Environ. Sci. Technol. XXXX, XXX, XXX−XXX

Table 2. Fitted Model Parameters Using Different Model Formulations[a]

Model	λ	d_{50} [μm]	k_{sw1} [min^{-1}]	k_{rs1} [min^{-1}]	S_{max1}/C_0 [cm^3 g^{-1}]	SE S_{max}/C_o	Column K_D [cm^3 g^{-1}]	Batch K_D [cm^3 g^{-1}]	Geometric S_f [%]	BET S_f [%]	R^2_{BTC}	R^2_{RP}
M1	0	350	0.053	3×10^{-03}	0.186	6.10×10^{-02}	4.29	0.3	0.32 ± 0.21	0.05 ± 0.03	0.968	0.621
M1	0.1	350	0.079	1×10^{-03}	0.634	0.13	18.59	1.22	1.08 ± 0.46	0.17 ± 0.07	0.991	0.732
M1	0.3	350	0.34	4×10^{-04}	12.17	1.93	213.74	3.06	22.03 ± 7.07	2.92 ± 0.94	0.993	0.985
M1	0.1	240	0.551	3×10^{-04}	4.342	0.46	NF	NF	5.14 ± 1.09	0.48 ± 0.10	0.976	0.994
M1	0.1	607	0.059	5×10^{-03}	0.289	4.20×10^{-02}	NF	NF	0.74 ± 0.21	0.52 ± 0.15	0.987	0.726

Model	λ	d_{50} [μm]	k_{sw1} [min^{-1}]	S_{max1}/C_0 [cm^3 g^{-1}]	k_{QS} [min^{-1}]	S_{maxQS}/C_0 [cm^3 g^{-1}]	k_{sw2} [min^{-1}]	S_{max2}/C_0 [cm^3 g^{-1}]	k_{GQS} [min^{-1}]	S_{maxGQS}/C_0 [cm^3 g^{-1}]	R^2_{BTC+RP}
M2	0	350	0.053	0.186	0.053	0.186	0	0	0.32	4.67	0.917
M2	0.1	350	0.047	0.167	0.053	0.186	0.032	0.47	0.32	4.67	0.867
M2	0.3	350	0.037	0.13	0.053	0.186	0.096	1.40	0.32	4.67	0.466

Model	λ	d_{50} [μm]	k_{sw1} [min^{-1}]	k_{rs1} [min^{-1}]	S_{max1}/C_0 [cm^3 g^{-1}]	k_{sw2} [min^{-1}]	k_{rs2} [min^{-1}]	β	R^2_{BTC}	R^2_{RP}
M3	0	350	0.059	NF	0.039	0.491	NF	0.765	0.971	0.986
M3	0.1	350	0.061	NF	0.151	0.817	NF	0.765	0.99	0.906
M3	0.3	350	0.309	NF	3.862	1.066	NF	0.765	0.991	0.958
M3	0.1	240	0.513	NF	4.665	0.907	NF	0.765	0.974	0.999
M3	0.1	607	0.032	NF	0.044	0.516	NF	0.765	0.987	0.995

[a] R^2_{BTC}, R^2_{RP}, and R^2_{BTC+RP} reflect the correlation of observed and fitted data for BTC, RP, and Total (BTC+PR), respectively. NF denotes not fitted. In M2 model, $k_{rs1} = k_{rs2} = 1\ E^{-5}$ min^{-1}; $k_{sw1} = (1 - \lambda)\ k_{QS}$, $k_{sw2} = \lambda\ k_{GQS}$, $S_{max1} = (1 - \lambda)\ S_{maxQS}$, $S_{max2} = \lambda\ S_{maxGQS}$, where k_{QS} and k_{GQS} are k_{sw} values for QS and GQS, respectively. S_{maxQS} and S_{maxGQS} are S_{max} values for QS and GQS, respectively.

electrostatic zone of influence, which is proportional to the colloid size.[65] In particular, the influence of nanoscale chemical heterogeneity is less pronounced for larger colloids because these effects are averaged over a larger zone of influence.[66,67]

MWCNT BTCs shown in Figure 2a exhibited time-dependent blocking behavior (increasing breakthrough concentrations with injection) as retention locations filled over time. Fitted values of S_{max1} increased with λ (Table 2) because of the presence of more electrostatically favorable goethite-coated retention locations. Time-dependent blocking behavior is less apparent in Figure 2a for higher values of S_{max1} because they take a long time to fill. Consequently, fitted values of S_{max1} exhibited a greater standard error at high values of $\lambda = 0.3$.

Table 2 shows fitted values of S_{max1} and the standard error that was used to calculate its 95% confidence interval. Table S1 provides geometric estimates and BET measurements for A_s. This information was used to calculate corresponding values of S_f with eq 5. Calculated values of S_f were very small. For example, when $\lambda = 0.1$, the 95% confidence interval for S_f was always <1.6%, even when goethite coated 10% of the sand surface. Equation 5 indicates that the value of S_f is inversely related to A_s. The BET value of A_s was much higher than the geometric value of A_s. Consequently, BET values of S_f were around 1 order of magnitude smaller than those based on geometric estimates of A_s. These low S_f values suggested that highly unfavorable attachment conditions occurred even on goethite-coated surfaces that are electrostatically favorable for attachment. An explanation for this observation is due to nanoscale roughness (Figures S1). The combined influence of nanoscale roughness and Born repulsion produces shallow primary minima (Figure S2),[30] and colloids that interact in these minima are susceptible to diffusive or hydrodynamic removal.[28,29]

The M2 model may be used to separately quantify the transport and retention of MWCNTs on QS and GQS sites. In this case, fitted values of k_{sw1} and S_{max1} from the M1 model were used to predict QS and GQS parameters for the M2 model by assuming a linear dependence on λ (Table 2). A summary of these calculated M2 model parameters is given in Table 2, as well as the R^2 values between observed and predicted BTCs and RPs. Predicted BTCs and RPs for the M2 model provided a much poorer description of the data than the fitted M1 model. This occurs because fitted M1 model parameters exhibited a nonlinear dependence on λ (Table 2). Consequently, information on the transport and retention parameters for the individual components is not sufficient to predict behavior of the sand mixture. However, M2 model parameters may still be fitted to BTCs for MWCNTs to give an equal or superior description of this data than the M1 model because of the increased number of fitting parameters.

Although the M1 model always described the BTCs very well, the RPs were poorly described when $\lambda = 0$ or 0.1 (cf., Figure 2b and Table 2). In these cases, the RPs exhibited a hyper-exponential shape, with MWCNT mass removal under predicted near the column inlet and overestimated at the column outlet. Interestingly, the BTC and RP were both well described when $\lambda = 0.3$. A number of potential explanations for hyper-exponential RPs have been provided in the literature, including straining,[40,68] chemical and/or size heterogeneity of the colloid suspension,[69,70] and pore-scale fluid distribution.[57,71] The relative importance of all of these factors on MWCNT retention cannot be conclusively deduced from the collected information. However, dramatic differences in batch and column scale retention indicate that surface straining played an important role in retention.

Additional terms need to be considered in the model to account for the observed depth-dependent retention shown in (Figure 2b). In particular, we employed a two-site retention model with time-dependent blocking on Site 1 and depth-dependent retention on Site 2 (M3 model). Simulated BTCs and RPs for the M3 model are also shown in Figure 2 and provide an excellent description of BTCs and RPs. The fitted model parameters and R^2 values are given in Table 2. As expected, the values of k_{sw1}, k_{sw2}, and S_{max1} increased with increasing λ. It should be mentioned that the relative importance of Sites 1 and 2 cannot be determined by comparison of the values of k_{sw1} and k_{sw2} because of the depth dependency on Site 2. However, model mass balance information can be used to determine the total amount and the fraction of retained MWCNTs that was

DOI: 10.1021/acs.est.6b03285
Environ. Sci. Technol. XXXX, XXX, XXX−XXX

associated with Sites 1 and 2. This information is shown in Table S2. The total amount associated with the depth-dependent site was relatively constant with λ (11.2%−18.9%). However, the fraction of retained MWCNTs that was associated with the depth-dependent site was much more important for lower values of λ, whereas the time-dependent site was dominant when λ = 0.3. Note that surface straining processes have been demonstrated to be more important under highly unfavorable attachment conditions.[28] This implies an association between the depth-dependent site and surface straining.

Effect of Grain Size on MWCNT Transport. Additional column experiments were conducted to investigate the transport and retention behavior of MWCNTs in porous media having the same value of λ = 0.1 but different grain sizes (240, 350, and 607 μm). Figure 3a and b shows the observed and simulated BTCs

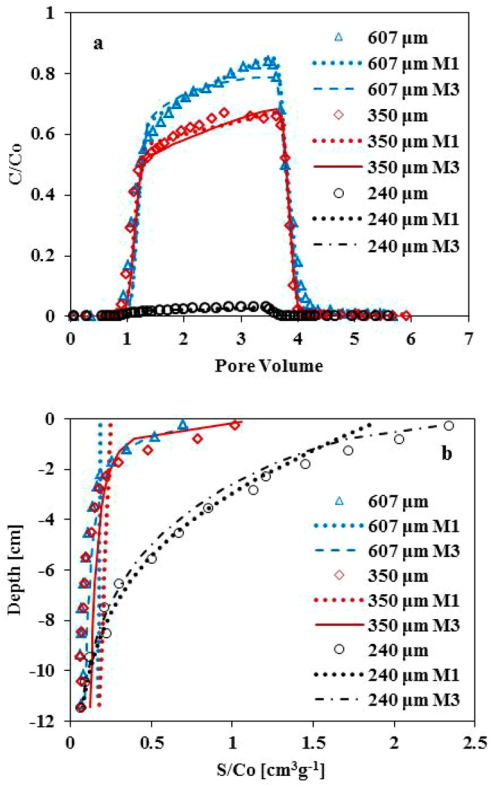

Figure 3. Observed and simulated breakthrough curves (a) and retention profiles (b) for MWCNTs in goethite-coated quartz sand with three different grain sizes (240, 350, and 607 μm) but the same λ (0.1). The Darcy velocity was 0.72−0.75 cm min^{-1}.

and RPs, respectively. The experimental conditions and mass balance information are summarized in Table 1. Fitted M1 and M3 model parameters and R^2 values for BTCs and RPs are shown in Table 2. The M_{total} was always greater than 90.7%. Values of M_{eff} and M_{solid} increased (2.4% to 76.0%) and decreased (94.2% to 17.7%), respectively, as the grain size increased from 240 to 607 μm. Similarly, fitted values of k_{sw1} when using the one site retention and blocking model (M1) increase in a nonlinear fashion with decreasing grain size. Colloid filtration theory predicts that this trend of increasing k_{sw1} and M_{solid} with decreasing grain size occurs because of an increasing rate of mass transfer to the solid surface.[11,53,72] Direct comparison of fitted and filtration theory predictions for k_{sw1} are hampered by the needle-like shape of the MWCNTs and the need to independently estimate the sticking efficiency.

Fitted values of S_{max1} from the M1 model also increased with decreasing grain size. This trend is expected because the surface area of the sand increases with decreasing grain size (Table S1), and this produces more electrostatically favorable sites for retention on the goethite-coated sand. The MWCNT BTCs exhibited some time-dependent blocking behavior in Figure 3. These blocking effects were more pronounced for increasing collector grain size because of smaller values of S_{max1}. As explained previously, corresponding values of S_f values were very small; for example, the 95% confidence interval on S_f was always less than 6.3% and 0.68% (Table 2) when using geometric estimates and BET measurement for A_s, respectively. This observation further supports the conclusion that only a small portion of the goethite coatings on the sand surface were favorable for retention.

The RPs shown in Figure 3b again exhibited a hyperexponential distribution with depth that was not well described using the one-site retention and blocking model (M1). The two-site model with time- (Site 1) and depth- (Site 2) dependent retention (M3) was used to simulate this behavior. Simulation results are shown in Figure 3, and fitted model parameters are given in Table 2. Values of k_{sw1}, k_{sw2}, and S_{max1} increased with decreasing grain size. The value of k_{sw1} was more sensitive to grain size than k_{sw2}, especially when the grain size decreased from 350 to 240 μm. In general, the value of k_{sw2} was relatively insensitive to λ because this parameter was mainly controlled by system hydrodynamics such as flow velocity and grain size distribution.[50]

Environmental Implications. Chemical heterogeneity of porous media surfaces is commonly assumed to control colloid transport and retention. Our results demonstrate that MWCNT retention in chemically heterogeneous porous media was controlled mainly by roughness but that the mass fraction and surface area (inversely related to the sand size) of chemical heterogeneity also played an important secondary role. Roughness and Born repulsion can diminish colloid retention on electrostatically favorable surfaces by creating shallow primary minimum interactions that are susceptible to removal by diffusion and hydrodynamic forces. Conversely, roughness can enhance retention on electrostatically unfavorable surfaces by locally reducing the energy barrier and increasing and decreasing the lever arms associated with adhesive and hydrodynamic torques, respectively, in column systems. Measured breakthrough curves and retentions profiles for MWCNTs exhibited time- and depth-dependent retention behavior even in the presence of significant fractions of goethite. This implies that simple, irreversible retention models to describe colloid retention in chemically heterogeneous soils may frequently be inadequate and that transport of colloids may be greater than expected.

■ ASSOCIATED CONTENT

Supporting Information

The Supporting Information is available free of charge on the ACS Publications website at DOI: 10.1021/acs.est.6b03285.

Details pertaining to porous media preparation and characterization (S1), interaction energy calculations (S2), and determination of S_f (S3). Figure S1 shows SEM images of QS and GQS. Figure S2 presents plots of $\Phi(h)$ when a spherical colloid approaches the surface of QS and GQS with different roughness properties in 1 mM KCl. Table S1 provides information on the sand surface

DOI: 10.1021/acs.est.6b03285
Environ. Sci. Technol. XXXX, XXX, XXX−XXX

area and iron content. Table S2 provides mass balance information for the M3 model. (PDF)

AUTHOR INFORMATION

Corresponding Author

*Phone: +1 951 369-4857. Fax: +1 951 342-4964. E-mail: scott.bradford@ars.usda.gov.

Notes

The authors declare no competing financial interest.

ACKNOWLEDGMENTS

M.Z. thanks the China Scholarship Council (CSC) for financial support. The authors also acknowledge the technical assistance from Stephan Köppchen, Brendan Headd, Claudia Walraf, Volker Nischwitz, Markus Duschl, and Herbert Philipp.

REFERENCES

(1) Iijima, S. Helical Microtubules of Graphitic Carbon. *Nature* **1991**, *354* (6348), 56−58.

(2) Mauter, M. S.; Elimelech, M. Environmental Applications of Carbon-Based Nanomaterials. *Environ. Sci. Technol.* **2008**, *42* (16), 5843−5859.

(3) Gannon, C. J.; Cherukuri, P.; Yakobson, B. I.; Cognet, L.; Kanzius, J. S.; Kittrell, C.; Weisman, R. B.; Pasquali, M.; Schmidt, H. K.; Smalley, R. E.; Curley, S. A. Carbon Nanotube-Enhanced Thermal Destruction of Cancer Cells in a Noninvasive Radiofrequency Field. *Cancer* **2007**, *110* (12), 2654−65.

(4) Gohardani, O.; Elola, M. C.; Elizetxea, C. Potential and Prospective Implementation of Carbon Nanotubes on Next Generation Aircraft and Space Vehicles: A Review of Current and Expected Applications in Aerospace Sciences. *Prog. Aerosp. Sci.* **2014**, *70*, 42−68.

(5) Gottschalk, F.; Sonderer, T.; Scholz, R. W.; Nowack, B. Modeled Environmental Concentrations of Engineered Nanomaterials (TiO_2, ZnO, Ag, CNT, Fullerenes) for Different Regions. *Environ. Sci. Technol.* **2009**, *43* (24), 9216−9222.

(6) Yang, J.; Bitter, J. L.; Smith, B. A.; Fairbrother, D. H.; Ball, W. P. Transport of Oxidized Multi-Walled Carbon Nanotubes through Silica Based Porous Media: Influences of Aquatic Chemistry, Surface Chemistry, and Natural Organic Matter. *Environ. Sci. Technol.* **2013**, *47* (24), 14034−14043.

(7) Lam, C.-W.; James, J. T.; McCluskey, R.; Hunter, R. L. Pulmonary Toxicity of Single-Wall Carbon Nanotubes in Mice 7 and 90 Days after Intratracheal Instillation. *Toxicol. Sci.* **2003**, *77* (1), 126−134.

(8) Lam, C.-w.; James, J. T.; McCluskey, R.; Arepalli, S.; Hunter, R. L. A Review of Carbon Nanotube Toxicity and Assessment of Potential Occupational and Environmental Health Risks. *Crit. Rev. Toxicol.* **2006**, *36* (3), 189−217.

(9) Farré, M.; Gajda-Schrantz, K.; Kantiani, L.; Barceló, D. Ecotoxicity and Analysis of Nanomaterials in the Aquatic Environment. *Anal. Bioanal. Chem.* **2009**, *393* (1), 81−95.

(10) Wang, Y.; Kim, J. H.; Baek, J. B.; Miller, G. W.; Pennell, K. D. Transport Behavior of Functionalized Multi-Wall Carbon Nanotubes in Water-Saturated Quartz Sand as a Function of Tube Length. *Water Res.* **2012**, *46* (14), 4521−31.

(11) Kasel, D.; Bradford, S. A.; Šimůnek, J.; Heggen, M.; Vereecken, H.; Klumpp, E. Transport and Retention of Multi-Walled Carbon Nanotubes in Saturated Porous Media: Effects of Input Concentration and Grain Size. *Water Res.* **2013**, *47* (2), 933−44.

(12) Kasel, D.; Bradford, S. A.; Šimůnek, J.; Pütz, T.; Vereecken, H.; Klumpp, E. Limited Transport of Functionalized Multi-Walled Carbon Nanotubes in Two Natural Soils. *Environ. Pollut.* **2013**, *180* (0), 152−158.

(13) Lu, Y.; Yang, K.; Lin, D. Transport of Surfactant-Facilitated Multiwalled Carbon Nanotube Suspensions in Columns Packed with Sized Soil Particles. *Environ. Pollut.* **2014**, *192*, 36−43.

(14) Mamedov, A. A.; Kotov, N. A.; Prato, M.; Guldi, D. M.; Wicksted, J. P.; Hirsch, A. Molecular Design of Strong Single-Wall Carbon Nanotube/Polyelectrolyte Multilayer Composites. *Nat. Mater.* **2002**, *1* (3), 190−194.

(15) Jaisi, D. P.; Elimelech, M. Single-Walled Carbon Nanotubes Exhibit Limited Transport in Soil Columns. *Environ. Sci. Technol.* **2009**, *43* (24), 9161−9166.

(16) Liu, X.; O'Carroll, D. M.; Petersen, E. J.; Huang, Q.; Anderson, C. L. Mobility of Multiwalled Carbon Nanotubes in Porous Media. *Environ. Sci. Technol.* **2009**, *43* (21), 8153−8158.

(17) Mattison, N. T.; O'Carroll, D. M.; Kerry Rowe, R.; Petersen, E. J. Impact of Porous Media Grain Size on the Transport of Multi-Walled Carbon Nanotubes. *Environ. Sci. Technol.* **2011**, *45* (22), 9765−75.

(18) Tian, Y.; Gao, B.; Wang, Y.; Morales, V. L.; Carpena, R. M.; Huang, Q.; Yang, L. Deposition and Transport of Functionalized Carbon Nanotubes in Water-Saturated Sand Columns. *J. Hazard. Mater.* **2012**, *213-214*, 265−72.

(19) Tian, Y.; Gao, B.; Wu, L.; Munoz-Carpena, R.; Huang, Q. Effect of Solution Chemistry on Multi-Walled Carbon Nanotube Deposition and Mobilization in Clean Porous Media. *J. Hazard. Mater.* **2012**, *231−232*, 79−87.

(20) Lu, Y.; Xu, X.; Yang, K.; Lin, D. The Effects of Surfactants and Solution Chemistry on the Transport of Multiwalled Carbon Nanotubes in Quartz Sand-Packed Columns. *Environ. Pollut.* **2013**, *182*, 269−77.

(21) Bradford, S.; Bettahar, M. Straining, Attachment, and Detachment of Oocysts in Saturated Porous Media. *J. Environ. Qual.* **2005**, *34* (2), 469−478.

(22) Jaisi, D. P.; Saleh, N. B.; Blake, R. E.; Elimelech, M. Transport of Single-Walled Carbon Nanotubes in Porous Media: Filtration Mechanisms and Reversibility. *Environ. Sci. Technol.* **2008**, *42* (22), 8317−8323.

(23) Parks, G. A. The Isoelectric Points of Solid Oxides, Solid Hydroxides, and Aqueous Hydroxo Complex Systems. *Chem. Rev.* **1965**, *65* (2), 177−198.

(24) Alvarez-Silva, M.; Uribe-Salas, A.; Mirnezami, M.; Finch, J. A. The Point of Zero Charge of Phyllosilicate Minerals Using the Mular−Roberts Titration Technique. *Miner. Eng.* **2010**, *23* (5), 383−389.

(25) Kim, S. B.; Park, S. J.; Lee, C. G.; Choi, N. C.; Kim, D. J. Bacteria Transport through Goethite-Coated Sand: Effects of Solution Ph and Coated Sand Content. *Colloids Surf., B* **2008**, *63* (2), 236−42.

(26) Foppen, J. W. A.; Schijven, J. F. Transport of E. Coli in Columns of Geochemically Heterogeneous Sediment. *Water Res.* **2005**, *39* (13), 3082−3088.

(27) Wang, D.; Bradford, S. A.; Harvey, R. W.; Gao, B.; Cang, L.; Zhou, D. Humic Acid Facilitates the Transport of ARS-Labeled Hydroxyapatite Nanoparticles in Iron Oxyhydroxide-Coated Sand. *Environ. Sci. Technol.* **2012**, *46* (5), 2738−2745.

(28) Bradford, S. A.; Torkzaban, S. Determining Parameters and Mechanisms of Colloid Retention and Release in Porous Media. *Langmuir* **2015**, *31* (44), 12096−12105.

(29) Torkzaban, S.; Bradford, S. A. Critical Role of Surface Roughness on Colloid Retention and Release in Porous Media. *Water Res.* **2016**, *88*, 274−284.

(30) Bradford, S. A.; Torkzaban, S. Colloid Interaction Energies for Physically and Chemically Heterogeneous Porous Media. *Langmuir* **2013**, *29* (11), 3668−3676.

(31) Bradford, S. A.; Torkzaban, S.; Leij, F.; Šimůnek, J. Equilibrium and Kinetic Models for Colloid Release under Transient Solution Chemistry Conditions. *J. Contam. Hydrol.* **2015**, *181*, 141−152.

(32) Treumann, S.; Torkzaban, S.; Bradford, S. A.; Visalakshan, R. M.; Page, D. An Explanation for Differences in the Process of Colloid Adsorption in Batch and Column Studies. *J. Contam. Hydrol.* **2014**, *164*, 219−229.

(33) Abraham, P. M.; Barnikol, S.; Baumann, T.; Kuehn, M.; Ivleva, N. P.; Schaumann, G. E. Sorption of Silver Nanoparticles to Environmental and Model Surfaces. *Environ. Sci. Technol.* **2013**, *47* (10), 5083−5091.

(34) Sadeghi, G.; Schijven, J. F.; Behrends, T.; Hassanizadeh, S. M.; van Genuchten, M. T. Bacteriophage Prd1 Batch Experiments to Study Attachment, Detachment and Inactivation Processes. *J. Contam. Hydrol.* **2013**, *152*, 12−17.

DOI: 10.1021/acs.est.6b03285
Environ. Sci. Technol. XXXX, XXX, XXX−XXX

(35) Shapiro, A.; Bedrikovetsky, P. A Stochastic Theory for Deep Bed Filtration Accounting for Dispersion and Size Distributions. *Phys. A* **2010**, *389* (13), 2473−2494.
(36) Bradford, S. A.; Torkzaban, S.; Leij, F.; Šimůnek, J.; van Genuchten, M. T. Modeling the Coupled Effects of Pore Space Geometry and Velocity on Colloid Transport and Retention. *Water Resour. Res.* **2009**, *45* (2), na.
(37) Leij, F. J.; Bradford, S. A. Combined Physical and Chemical Nonequilibrium Transport Model: Analytical Solution, Moments, and Application to Colloids. *J. Contam. Hydrol.* **2009**, *110* (3), 87−99.
(38) Cherrey, K. D.; Flury, M.; Harsh, J. B. Nitrate and Colloid Transport through Coarse Hanford Sediments under Steady State, Variably Saturated Flow. *Water Resour. Res.* **2003**, *39* (6), n/a.
(39) Harvey, R. W.; Garabedian, S. P. Use of Colloid Filtration Theory in Modeling Movement of Bacteria through a Contaminated Sandy Aquifer. *Environ. Sci. Technol.* **1991**, *25* (1), 178−185.
(40) Bradford, S. A.; Šimůnek, J.; Bettahar, M.; van Genuchten, M. T.; Yates, S. R. Modeling Colloid Attachment, Straining, and Exclusion in Saturated Porous Media. *Environ. Sci. Technol.* **2003**, *37* (10), 2242−2250.
(41) Bradford, S. A.; Torkzaban, S.; Šimůnek, J. Modeling Colloid Transport and Retention in Saturated Porous Media under Unfavorable Attachment Conditions. *Water Resour. Res.* **2011**, *47* (10), n/a.
(42) Schijven, J. F.; Hassanizadeh, S. M. Removal of Viruses by Soil Passage: Overview of Modeling, Processes, and Parameters. *Crit. Rev. Environ. Sci. Technol.* **2000**, *30* (1), 49−127.
(43) Corapcioglu, M. Y.; Choi, H. Modeling Colloid Transport in Unsaturated Porous Media and Validation with Laboratory Column Data. *Water Resour. Res.* **1996**, *32* (12), 3437−3449.
(44) Camesano, T. A.; Unice, K. M.; Logan, B. E. Blocking and Ripening of Colloids in Porous Media and Their Implications for Bacterial Transport. *Colloids Surf., A* **1999**, *160* (3), 291−307.
(45) Bradford, S. A.; Wang, Y.; Kim, H.; Torkzaban, S.; Šimůnek, J. Modeling Microorganism Transport and Survival in the Subsurface. *J. Environ. Qual.* **2014**, *43* (2), 421−40.
(46) Pauluhn, J. Multi-Walled Carbon Nanotubes (Baytubes®): Approach for Derivation of Occupational Exposure Limit. *Regul. Toxicol. Pharmacol.* **2010**, *57* (1), 78−89.
(47) Kim, S.; Mulholland, G.; Zachariah, M. Density Measurement of Size Selected Multiwalled Carbon Nanotubes by Mobility-Mass Characterization. *Carbon* **2009**, *47* (5), 1297−1302.
(48) Scheidegger, A.; Borkovec, M.; Sticher, H. Coating of Silica Sand with Goethite: Preparation and Analytical Identification. *Geoderma* **1993**, *58* (1), 43−65.
(49) Brunauer, S.; Emmett, P. H.; Teller, E. Adsorption of Gases in Multimolecular Layers. *J. Am. Chem. Soc.* **1938**, *60* (2), 309−319.
(50) Wang, D.; Bradford, S. A.; Paradelo, M.; Peijnenburg, W. J.; Zhou, D. Facilitated Transport of Copper with Hydroxyapatite Nanoparticles in Saturated Sand. *Soil Sci. Am. J.* **2012**, *76* (2), 375−388.
(51) Mekonen, A.; Sharma, P.; Fagerlund, F. Transport and Mobilization of Multiwall Carbon Nanotubes in Quartz Sand under Varying Saturation. *Environ. Earth Sci.* **2014**, *71* (8), 3751−3760.
(52) OECD. *Test No. 106: Adsorption -- Desorption Using a Batch Equilibrium Method*; OECD Publishing: Paris, 2000.
(53) Liang, Y.; Bradford, S. A.; Šimůnek, J.; Vereecken, H.; Klumpp, E. Sensitivity of the Transport and Retention of Stabilized Silver Nanoparticles to Physicochemical Factors. *Water Res.* **2013**, *47* (7), 2572−2582.
(54) Gottschalk, F.; Sun, T.; Nowack, B. Environmental Concentrations of Engineered Nanomaterials: Review of Modeling and Analytical Studies. *Environ. Pollut.* **2013**, *181* (0), 287−300.
(55) Šimůnek, J.; Genuchten, M. T. v.; Šejna, M. Recent Developments and Applications of the Hydrus Computer Software Packages. *Vadose Zone J.* **2016**, *15*, 0.
(56) Schijven, J. F.; Šimůnek, J. Kinetic Modeling of Virus Transport at the Field Scale. *J. Contam. Hydrol.* **2002**, *55* (1−2), 113−135.
(57) Wang, D.; Paradelo, M.; Bradford, S. A.; Peijnenburg, W. J. G. M.; Chu, L.; Zhou, D. Facilitated Transport of Cu with Hydroxyapatite Nanoparticles in Saturated Sand: Effects of Solution Ionic Strength and Composition. *Water Res.* **2011**, *45* (18), 5905−5915.
(58) Johnson, P. R.; Elimelech, M. Dynamics of Colloid Deposition in Porous Media: Blocking Based on Random Sequential Adsorption. *Langmuir* **1995**, *11* (3), 801−812.
(59) Duschl, M.; Pohlmeier, A.; Brox, T. I.; Galvosas, P.; Vereecken, H. Effect of Magnetic Pore Surface Coating on the NMR Relaxation and Diffusion Signal in Quartz Sand. *Magn. Reson. Chem.* **2016**, DOI: 10.1002/mrc.4486.
(60) Hofmann, A.; Liang, L. Mobilization of Colloidal Ferrihydrite Particles in Porous Media—an Inner-Sphere Complexation Approach. *Geochim. Cosmochim. Acta* **2007**, *71* (24), 5847−5861.
(61) Wang, D.; Zhang, W.; Zhou, D. Antagonistic Effects of Humic Acid and Iron Oxyhydroxide Grain-Coating on Biochar Nanoparticle Transport in Saturated Sand. *Environ. Sci. Technol.* **2013**, *47* (10), 5154−5161.
(62) Jin, Y.; Yates, M. V.; Thompson, S. S.; Jury, W. A. Sorption of Viruses During Flow through Saturated Sand Columns. *Environ. Sci. Technol.* **1997**, *31* (2), 548−555.
(63) Praetorius, A.; Tufenkji, N.; Goss, K.-U.; Scheringer, M.; von der Kammer, F.; Elimelech, M. The Road to Nowhere: Equilibrium Partition Coefficients for Nanoparticles. *Environ. Sci.: Nano* **2014**, *1* (4), 317−323.
(64) Elimelech, M.; Nagai, M.; Ko, C.-H.; Ryan, J. N. Relative Insignificance of Mineral Grain Zeta Potential to Colloid Transport in Geochemically Heterogeneous Porous Media. *Environ. Sci. Technol.* **2000**, *34* (11), 2143−2148.
(65) Duffadar, R. D.; Davis, J. M. Dynamic Adhesion Behavior of Micrometer-Scale Particles Flowing over Patchy Surfaces with Nanoscale Electrostatic Heterogeneity. *J. Colloid Interface Sci.* **2008**, *326* (1), 18−27.
(66) Bradford, S. A.; Torkzaban, S. Colloid Adhesive Parameters for Chemically Heterogeneous Porous Media. *Langmuir* **2012**, *28* (38), 13643−13651.
(67) Bendersky, M.; Davis, J. M. DLVO Interaction of Colloidal Particles with Topographically and Chemically Heterogeneous Surfaces. *J. Colloid Interface Sci.* **2011**, *353* (1), 87−97.
(68) Bradford, S. A.; Yates, S. R.; Bettahar, M.; Šimůnek, J. Physical Factors Affecting the Transport and Fate of Colloids in Saturated Porous Media. *Water Resour. Res.* **2002**, *38* (12), 63-1.
(69) Tufenkji, N.; Elimelech, M. Spatial Distributions of Cryptosporidium Oocysts in Porous Media: Evidence for Dual Mode Deposition. *Environ. Sci. Technol.* **2005**, *39* (10), 3620−3629.
(70) Tong, M.; Johnson, W. P. Colloid Population Heterogeneity Drives Hyperexponential Deviation from Classic Filtration Theory. *Environ. Sci. Technol.* **2007**, *41* (2), 493−499.
(71) Bradford, S. A.; Kim, H. N.; Haznedaroglu, B. Z.; Torkzaban, S.; Walker, S. L. Coupled Factors Influencing Concentration-Dependent Colloid Transport and Retention in Saturated Porous Media. *Environ. Sci. Technol.* **2009**, *43* (18), 6996−7002.
(72) Sasidharan, S.; Torkzaban, S.; Bradford, S. A.; Dillon, P. J.; Cook, P. G. Coupled Effects of Hydrodynamic and Solution Chemistry on Long-Term Nanoparticle Transport and Deposition in Saturated Porous Media. *Colloids Surf., A* **2014**, *457*, 169−179.

DOI: 10.1021/acs.est.6b03285
Environ. Sci. Technol. XXXX, XXX, XXX−XXX